



Influence of Al grain structure on Fe bearing intermetallics during DC casting of an Al-Mg-Si alloy

S. Kumar^{*}, K.A.Q. O'Reilly

Department of Materials, University of Oxford, Parks Road, Oxford OX1 3PH, UK

ARTICLE INFO

Article history:

Received 6 May 2016

Received in revised form 9 September 2016

Accepted 12 September 2016

Available online 13 September 2016

Keywords:

Direct-chill casting

Aluminium alloys

Grain refinement

Solidification microstructure

Intermetallic phase selection

ABSTRACT

207 mm diameter direct chill (DC) cast billets of 6063 aluminium-magnesium-silicon (Al-Mg-Si) alloy were produced with various different primary aluminium (α -Al) grain structures including feathery-dendrites, equiaxed-dendrites and equiaxed-globular morphologies. To control the α -Al grain structure (grain morphology and grain size) an intensive shearing melt conditioning technique and Al-5Ti-1B grain refiner were used. For the first time, due to the variety of controlled microstructures produced in the DC billets, it was possible to study and determine the role of the α -Al grain structure on the iron (Fe) bearing intermetallics (Fe-IMCs). The size, shape and three dimensional (3D) inter-connectivity of the Fe-IMCs were observed to be affected by the modification of the primary α -Al grain morphology and grain size. Although both " α -AlFeSi" and " β -AlFeSi" phases are present in all billets, β -AlFeSi phase is dominant in the billets with grain refiner addition while α -AlFeSi is dominant in the billets without grain refiner. This suggests that the addition of Al-5Ti-1B grain refiner plays a more significant role in the intermetallic phase selection than the primary α -Al grain morphology or grain size.

© 2016 Elsevier Inc. All rights reserved.

1. Introduction

Wrought AA6xxx series Al alloys are typically produced in either an ingot or billet form using direct chill (DC) casting, and are suitable for manufacturing roll or extruded products [1]. The appearance and performance of products formed from DC cast billet depends on the nature of "in-soluble" secondary phase particles (particularly Fe-IMCs) present in the as-cast microstructure [2–5]. To produce final products, the cast billet is usually subjected to different downstream processes, such as heat treatment, extrusion and rolling [6–9]. Our previous research revealed that the type, size and distribution of the Fe-IMCs in the final processed product strongly depends on their features in the as-cast billets [10–12]. The as-cast IMC particle features also dictate whether a pre-heat-treatment step is required for successful rolling/extrusion [12]. Therefore it is essential to understand and control the IMCs during solidification.

It has been well documented in published literature that the nature of Fe-IMCs in dilute Al alloys is affected by solidification processing conditions such as cooling rate, thermal gradient, growth velocity, trace elements and Al grain refiner [13–19]. Researchers [20–24] have argued that the change in primary α -Al grain morphology and grain size, caused by successful grain refinement, played a role in intermetallic phase selection in Al alloys containing grain refiner additions. It was

proposed [20–24] that to accommodate such convoluted liquid shapes in the grain refined samples, the Fe-IMCs, which can nucleate and branch easily, will be favoured. Most of these solidification studies were conducted using laboratory scale equipment, such as Bridgman directional solidification, rapid melt spinning or a DC simulator. To our knowledge, there is no published report available to show the individual effects of primary α -Al grain size, grain morphology and grain refiner addition on the intermetallic phase selection during solidification. Since the addition of grain refiner inherently reduces the grain size and alters the grain morphology, it is difficult to differentiate individual effects on the phase selection. Thus for the first time, we have systematically studied these individual effects on near industrial scale DC cast billets. This study will therefore be useful for industry to optimize their existing casting practice and to develop advanced solidification casting technologies [10,25–32] e.g. to produce billet (using complex alloys from recycled materials) with more favourable microstructures for better downstream processing yielding good quality end products.

In this paper, billets with different α -Al structures were produced by DC casting an AA6063 Al alloy without and with (i) applying intensive melt shearing, and (ii) commercial Al-5Ti-1B grain refiner addition. An intermetallic phase extraction technique was used to evaluate the chemical and structural nature of the intermetallic phases and to reveal the changes in the 3D morphology, size and inter-connectivity between the network. From all of the studied conditions, it is clear that the addition of TiB₂ based grain refiner plays a key role in the intermetallic phase selection, while the primary α -Al grain structure is shown to play a key role in the IMC particle size, shape and inter-connectivity.

^{*} Corresponding author.

E-mail address: kumar.sundaram@materials.ox.ac.uk (S. Kumar).

2. Experimental Details

Billets studied in this work were cast in a pilot-scale DC casting facility at the University of Oxford. The 6063 Al alloy used in this work was prepared in-house by adding appropriate amounts of Al-80Fe, Al-80Mn and Al-50Si master alloys (units in wt.% and hear after, unless otherwise stated), and high purity Mg and commercial purity (CP) Al. A gas fired tilting melting furnace was used to produce ~250 kg of the alloy. Once the CP Al reached ~750 °C the preheated alloying additions were added. A small amount of the melt was cast in a mushroom mould for chemical analysis. The nominal chemical composition, measured using a Spectrolab LAVFA05A spark analyser optical emission spectrometer, is given in Table 1.

The molten alloy was transferred via a ceramic launder system to feed the Oxford DC caster to produce 203 mm (8 in.) diameter and 2000 mm long billets. The parameters of the DC caster were kept uniform for these experiments: with start cast speed at 70 mm/min, run cast speed of 110 mm/min and water flow at 240 l/min. For the grain refiner addition experiments, when the billet length was about 1100 mm, a commercial Al-5Ti-1B grain refiner rod was introduced into the liquid metal via the launder system at a rate of approximately 1 ppm and the remaining billet length was cast with grain refiner. For simplicity, the billet portions cast without grain refiner are called NGR and the billet portions cast with grain refiner are called GR. For the intensive melt shearing experiments, a rotor-stator melt conditioning apparatus developed by Brunel University [33] was incorporated in the Oxford DC caster by placing it in the top of the launder head. Details of the melt shearing experiments are reported elsewhere [29]. The intensive melt sheared billets were also cast without and with Al-5Ti-1B grain refiner. For this study, the intensively sheared samples were taken from the billets discussed elsewhere [29].

The billets were cross-sectioned horizontally across the diameter for microstructural analysis. The results presented here were analysed at a position 80 mm from the billet outer edge. Metallography samples were prepared by mounting, grinding and polishing (diamond paste and colloidal silica). Samples were also anodized with Barkers reagent [7 ml HBF₄ (48 pct) and 93 ml H₂O] for 60 s at 20 V and studied by light microscopy (Zeiss Axiophot2) under polarised light and dark field imaging conditions, to assess the primary Al grain size and secondary phases. The mean linear intercept method was used to measure the primary α -Al grain size.

An intermetallic extraction apparatus (IEA) was used to extract the intermetallic particles from the as-cast samples, using a procedure similar to that reported in [34,35]. The IEA uses boiling anhydrous butan-1-ol (butanol) to dissolve the Al matrix of the alloy without reacting with the intermetallic phases. The intermetallic particles are then collected on a polytetrafluoroethylene (PTFE) filter membrane (47 mm diameter, 0.2 μ m pore size). The phases were identified using a Philips 1700 X-ray diffractometer (XRD) with Cu-K α (λ = 1.54 Å) source operated at 35 kV, 50 mA and 0.05° step size. A calibration procedure developed in house was used for determining the relative weight fractions of α -AlFeSi and β -AlFeSi from XRD data, more details of which can be found in references [16,18].

The metallographic samples and extracted particles were further analysed using different analytical scanning electron microscopes (SEM) including a JEOL 840F, JEOL 5510 and Zeiss Merlin, each equipped with secondary electron (SE) detector, backscattered electron (BSE)

detector, and energy dispersive spectrometer (EDS). Electron probe micro-analysis (EPMA) was also performed using a JEOL 8800 SEM equipped with wavelength dispersive spectrometers (WDS). MTDATA studio 5.10 software with NPL aluminium database V6.1 was used to predict phases as a function of temperature.

3. Results

3.1. Primary α -Al Grain Structure Analysis

Fig. 1 shows the microstructures of the four billets and the observed α -Al grain features are tabulated in Table 2 for all the melt treatments investigated. The secondary dendrite arm spacing (DAS) of NGR-FD, NGR-DG and GR-ED (terms as given in Table 2) are $27 \pm 8 \mu$ m. Overall, the addition of GR or intensive melt shearing or a combination of both reduced the primary α -Al grain size and modified the grain morphology.

Each feathery grain is bounded by straight (S in Fig. 1(a)) and ragged (R in Fig. 1(a)) boundaries. The straight and ragged boundaries are the result of coherent crystallographic twinning of the primary dendrite trunk [36] and dendrite impingement, respectively. As is well known [37], the columnar feathery structure forms when the liquid adjacent to the solidification front experiences (a) the absence of heterogeneous nucleation substrates for α -Al, (b) the presence of solute elements such as Si and Mg, and (c) a high thermal gradient. Similarly, the presence of the heterogeneous nucleation substrates suppresses the growth of the columnar crystals and more equiaxed grains are produced as shown in Fig. 1(c, d) of the GR samples.

The formation of fine equiaxed grains, as shown in Fig. 1(b) for the melt sheared sample is complex. Intensive shearing of the liquid metal ahead of the solid-liquid interfaces creates an environment with a high number of potent nucleating substrates, such as fragmented dendrite arms [38] or well dispersed naturally occurring intrinsic oxide particles [39], that nucleate the α -Al crystals and allow them to grow as equiaxed grains in the liquid whose temperature and composition are more uniform [29].

The presence of globular equiaxed structures seen in the intensively sheared GR sample in Fig. 1(d) suggest a possible planar mode of crystal growth [40], where the solute diffusion field around the floating growing grains was removed periodically by the forced turbulent liquid flow induced by the melt shearing. One grain with dual morphologies is clearly seen in Fig. 1(b) and marked as D. The centre of the grain has the globular morphology but it becomes dendritic towards the top and left of the grain. This is possible because the local equilibrium between the globular crystal and the surrounding liquid breaks down which occurs when the liquid convection is not effective enough to remove the diffusion field so leading to the dendritic growth mode.

3.2. Fe-IMCs Analysis

3.2.1. Location with Respect to the Primary α -Al Grain Morphology

In the case of grains with dendritic morphology the Fe-IMCs are located at the grain boundaries and within the grain envelopes (inter-dendritic region) (Fig. 1(e, g)), whereas in the grains with globular morphology the Fe-IMCs are located at the grain boundaries (inter-granular region) (Fig. 1(f, h)). The particles at the grain boundaries have a larger aspect ratio compared to the ones within the grain envelopes. The larger aspect ratio particles mainly have needle-like and script-like morphologies while the smaller aspect ratio particles mainly have rosette-like geometries, similar to those reported in Ref [41,42]. For a given area, the feathery dendritic grains have a larger proportion of the smaller aspect ratio Fe-IMCs particles. No Fe-IMCs particles can be found on the straight boundaries (S in Fig. 1(a, e)) of the feathery grains, which contrasts that reported in the Al-Zn alloy system [43,44].

Table 1
Nominal compositions of different batches of 6063 Al alloy prepared in this study.

Batch	Billet	Mg wt.%	Si	Fe	Mn	Ti	Al
1	Conventional NGR and GR	0.38	0.41	0.21	0.01	0.005	Balance
2	Intensive shear	0.38	0.38	0.18	0.01	0.002	Balance
3	Intensive sheared with GR	0.45	0.45	0.21	0.01	0.005	Balance

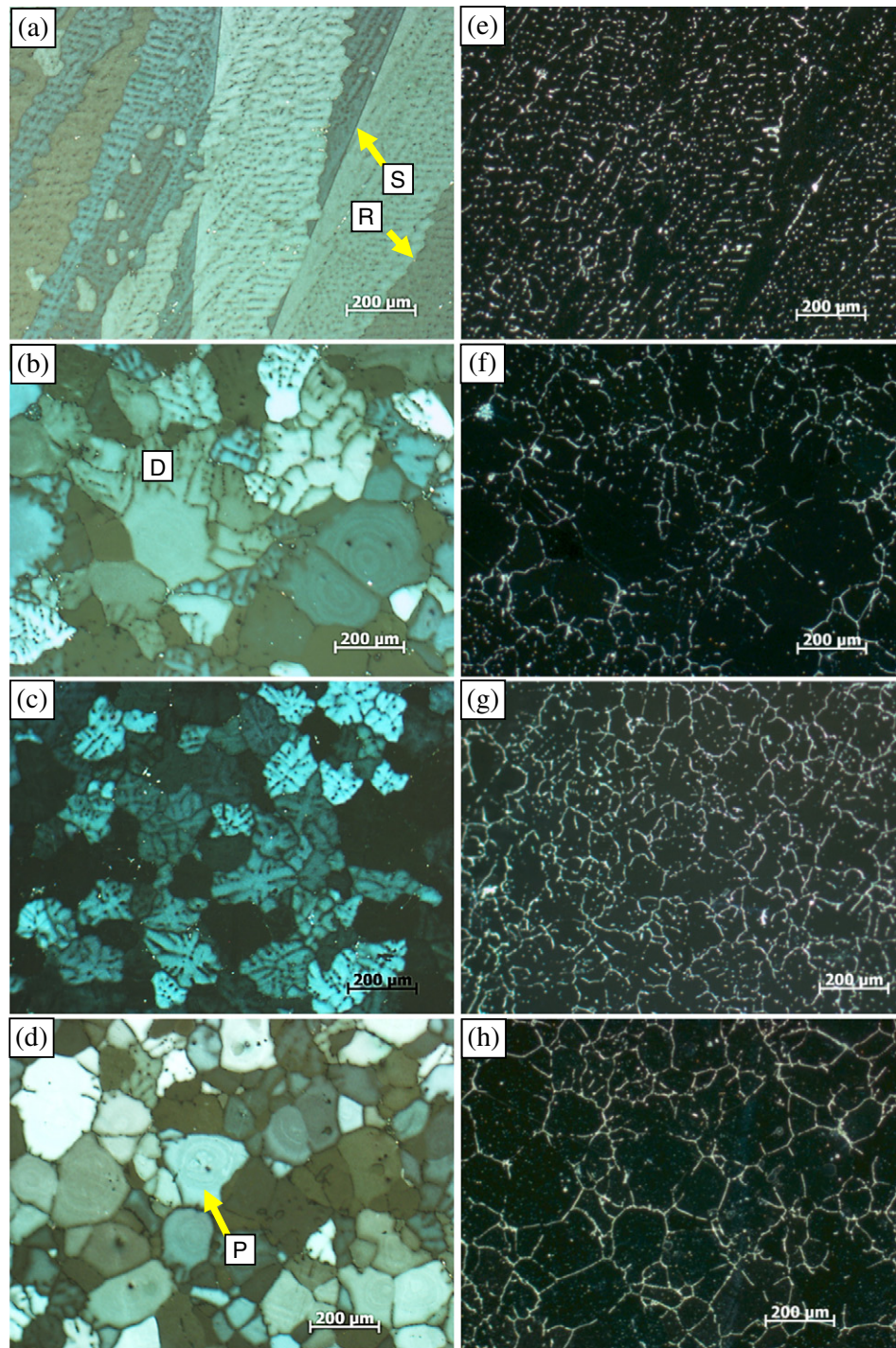


Fig. 1. Polarised (a, b, c, d) and dark field (e, f, g, h) light microscopy images showing different α -Al grain morphologies and corresponding positions of the secondary phases in the same area. Where (a, e) are from the NGR sample, (b, f) are from the intensively melt sheared NGR sample, (c, g) are from the GR sample and (d, h) are from the intensively melt sheared GR sample.

Table 2

Observed features in the four different samples.

Type of melt condition used	Morphology of primary α -Al grain	Grain size (μm)	Predominant Fe-IMCs	Predominant Fe-IMCs morphology	IMCs inter-connectivity
No melt condition	Columnar feathery dendrites (NGR-FD)	$> 10,000$	α_c -AlFeSi	Skeleton-like and spherical-like	Less
Intensive sheared	Mixed equiaxed dendrites and globular (NGR-DG)	167 ± 8	α_c -AlFeSi	Coarse petal/dendrite-like	Nearly high
Al-5Ti-1B	Equiaxed dendrites (GR-ED)	100 ± 8	β -AlFeSi	Platelet-like	High
Intensive sheared with Al-5Ti-1B	Mostly equiaxed globular (GR-G)	111 ± 18	β -AlFeSi	Platelet-like	High

3.2.2. Phase Identification and Quantification

The XRD patterns from the extracted particles, shown in Fig. 2(a), reveal the presence of cubic α -AlFeSi (for simplicity, α -Al(FeMn)Si is denoted as α -AlFeSi hereafter), monoclinic β -AlFeSi and cubic Mg_2Si in all of the billets. Of the Fe-IMCs, α -AlFeSi showed the highest intensity peaks in the NGR samples, whereas β -AlFeSi showed the highest intensity peaks in the GR samples. The phase fractions, analysed using calibration standards, are shown in Fig. 2(b), and suggest that in the NGR samples, the proportion of α -AlFeSi relative to β -AlFeSi is high (>75%), while in the GR samples, the proportion of α -AlFeSi is low (<27%). Even after significant refinement and modification of the α -Al grain structure using intensive melt shearing, α -AlFeSi was still the dominant phase in the NGR sample. The XRD analysis further confirms that formation of β -AlFeSi is promoted by the addition of Al-5Ti-1B grain refiner and this agrees well with Bridgman [15] and Rheo-cast [18] experiments. Overall, the present results confirm that the intermetallic phase selection is primarily governed by the addition of Al-5Ti-1B grain refiner in AA6063 melts, and not by reducing the grain size or modifying the primary α -Al grain morphology.

3.2.3. IMCs Inter-Connectivity, Morphology and Size

SEM analysis of the extracted particles revealed that the IMC particles present at the grain boundaries in the NGR-FD structure have poor 3D inter-connectivity (Fig. 3(a)) as the particles were more discrete, whereas the NGR-DG, GR-ED and GR-G samples resulted in sponge-like connected particles suggesting networks of highly inter-connected Fe-IMCs (Fig. 3(b, c, d)). Low magnification imaging of the GR-G sample in Fig. 3(e) shows a typical example of an extended network of highly inter-connected Fe-IMCs which appeared sponge-like. The voids inside the sponge represent the positions of the α -Al grains, and the shape of the voids is dictated by the α -Al grain morphology. The samples with globular α -Al (NGR-G and GR-G) show a distinct

periodic void pattern in the sponge as shown in Fig. 3(d) and Fig. 3(e). High magnification imaging revealed that the 3D network contained dendritic/petal-like particles or platelet-like particles or a combination of both. Closer examination of the contact point (Fig. 3(f)) of the combined particles revealed that both particles were nucleated separately, and then grew and impinged on each other to form a connection between them.

The NGR-FD sample, where α -AlFeSi was dominant, mostly had skeleton-like and spherical-like Fe-IMCs particles (Fig. 3(a)). The NGR-G sample, where α -AlFeSi was dominant, mostly had coarse dendrite/petal-like particles (Fig. 3(b)). Both the GR-ED and GR-G samples, where β -AlFeSi was dominant, mostly had platelet-like and rack-like particles (Fig. 3(c, d)). The flower-like particles (Fig. 4(a)) are also seen in NGR-DG, GR-ED and GR-G samples. These particles have six-petals and their centre always contain either oxides (Fig. 4(b, c)) or TiB_2 (Fig. 4(d)) particles suggesting that the nucleation occurred at these points with the petals growing outward thereafter. TiB_2 , oxide, Si and Mg_2Si particles were also observed to be associated with the platelet-like particles, as shown in Fig. 5 and Fig. 6. The Mg_2Si and platelet associations were similar to that reported in Fig. 11 of [42]. It is important to note that the dendrite-like and platelet-like Fe-IMCs particles are in all the samples, but their proportions varied. In accordance with our earlier studies [17,18,41,42] and with the present results, it is now clear that the α -AlFeSi particles have petal-like, dendrite-like, flower-like, skeleton-like and spherical-like morphologies, while the β -AlFeSi particles have platelet-like and rack-like morphologies. The dominant Fe-IMCs type, shape, and inter-connectivity with respect to different microstructures are summarised in Table 2.

The spherical-like particles (as in Fig. 12 of [42]) are the smallest aspect ratio particles that are observed within the grain envelope of the dendritic grains (Fig. 1). This suggests that the coarser the dendritic grains the larger the proportion of the spherical-like particles. A detailed study of the spherical-like Fe-IMCs particles and Mg_2Si in the DC cast billet of a similar alloy is reported elsewhere [42].

3.3. Distribution of Elements in the Cast Microstructures

EPMA mapping (Figs. 7 and 8) and line scan (Fig. 9) revealed that the concentrations of solute in the inter-dendritic and inter-granular regions are rich in Fe, Si and Mg, whereas Ti was richer inside the α -Al dendrites. In addition, the concentrations of solute in the solid solution of the α -Al dendrites nearer to the Fe-IMCs are rich in Mg and Si. This suggests that the Fe-IMCs form from liquid films rich in Mg, Si, Fe and Al elements. The ring-like patterns inside the globular grains in the polarised light microscopy image (denoted P in Fig. 1(d)) are due to enrichment and depletion of solute Ti, as seen in Figs. 7(c) and 8, which supports the argument of a planar growth mode for the globular crystals with intensive shearing. The bright spots in the Ti maps (e.g. circled) and high intensity peaks of Ti in the line scan correspond to the TiB_2 particles originating from the grain refiner addition, as the Al_3Ti particles present in the grain refiner master alloy would have dissolved after its addition to the base alloy. The TiB_2 particles are at the inter-dendritic and inter-granular locations and within the primary α -Al grains. Fig. 7(c) shows that the intensive melt sheared GR sample, had small sized Ti-rich inoculant clusters dispersed uniformly across the sample. Evidence of more Ti-rich particles/clusters inside the globular grains suggests possible engulfment during the primary α -Al growth suggesting wetting of the particles by the liquid.

3.4. Thermodynamic Phase Prediction

Thermodynamic simulations, using MTDATA under Scheil assumptions (i.e. no diffusion in the solid and complete mixing in the liquid states), were conducted for the alloy composition used in batch 1, as given in Table 1. The simulation predicted the formation of α -Al, $\text{Al}_{13}\text{Fe}_4$, α -AlFeSi, β -AlFeSi, Mg_2Si , α -AlMnSi and Si in this sequence

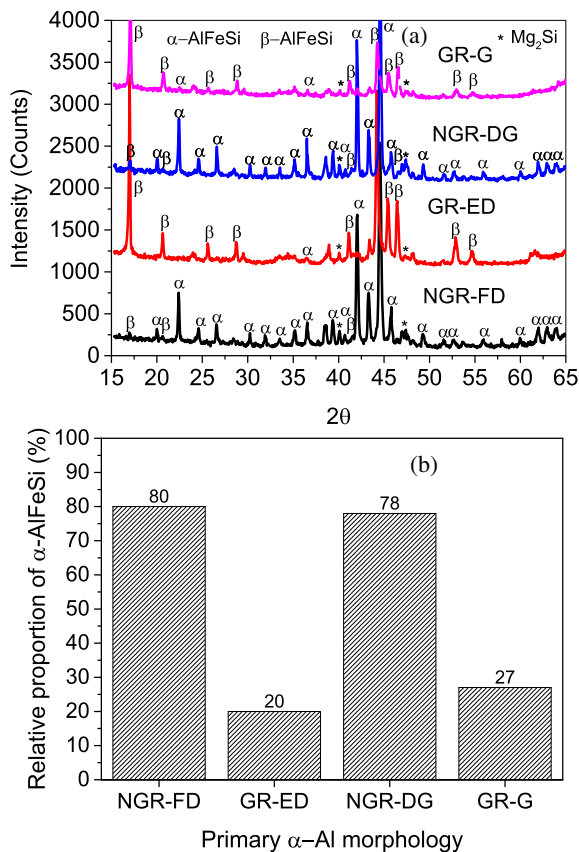


Fig. 2. (a) XRD patterns from the extracted particles formed in samples with different primary α -Al morphologies, and (b) their corresponding relative proportions of α -AlFeSi.

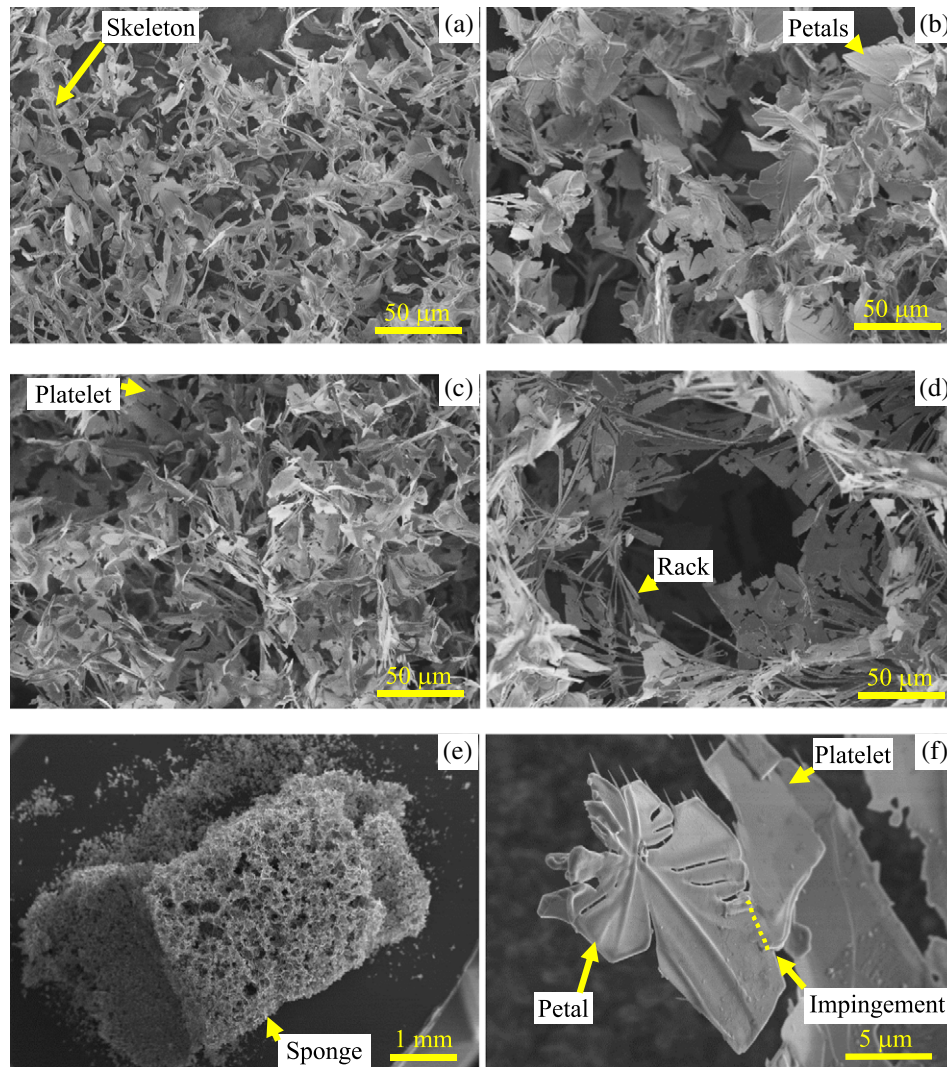


Fig. 3. FEG-SEM images of the extracted particles from samples with different primary α -Al morphologies. Where (a), (b), (c), (d) are from NGR-FD, NGR-DG, GR-ED, and GR-G samples, respectively, (e) shows the highly inter-connected “sponge-like” extracted particle structure (from GR-G), and (f) shows the contact point of petal-like and platelet-like particles. The dashed line in (f) shows the edge of the petal-like particle.

from the liquid, with decreasing temperature, as shown in Fig. 10(a). The thermodynamic calculations, under conditions where $\text{Al}_{13}\text{Fe}_4$ is suppressed, were performed by removing it from the candidate phase list and the predicted results obtained are as given in Fig. 10(b). This shows an increase in the α -AlFeSi formation temperature and fraction while β -AlFeSi, Mg_2Si , α -AlMnSi and Si solidify at the temperatures and fractions similar to that predicted in Fig. 10(a). Suppressing $\text{Al}_{13}\text{Fe}_4$ and α -AlFeSi, achieved by removing both from the candidate phase list, predicted that both β -AlFeSi and Mg_2Si formed at higher temperatures with larger phase fractions, as shown in Fig. 10(c). However, α -AlMnSi and Si still solidify at temperatures and phase fractions similar to those predicted in Fig. 10(b).

4. Discussion

From our present and previous investigations of the 6063 Al alloy [17,18,41,42], it can be concluded that the Fe-IMCs particles solidify either in the inter-dendritic region (within the grain envelope) or in the inter-granular region (at grain boundaries) or both, i.e. where the solute elements segregate during solidification, depending on the morphology of the primary α -Al that forms during casting. The Fe-IMCs form later in the solidification after the primary α -Al. The observed variations in the Fe-IMCs will be explained with respect to the nucleation and

growth of the primary α -Al and the Fe-IMCs particles. Fig. 11 illustrates schematically snapshots of solidifying 6063 billets during DC casting for different primary α -Al morphologies.

4.1. From the Perspective of the Primary α -Al Solidification

4.1.1. Concerning the Primary α -Al Nucleation

The addition of Al-5Ti-1B grain refiner to an Al alloy reduces the undercooling required to nucleate the primary α -Al by increasing the α -Al nucleation temperature [37]. The α -Al crystals that form at a high nucleation temperature will exhibit a higher purity and will have less solute in the solid solution, as the main solute elements such as Si and Mg have partition coefficients (k) < 1 and will therefore segregate into the liquid. This enrichment of solute in the remaining liquid continues as the solidification front proceeds. This can be understood from the binary Al-Si phase diagram: the equilibrium solidification of 0.41 wt.% Si starts at 657.8 °C and forms primary α -Al containing 0.043 wt.% Si. Assuming the alloy had undergone a nucleation undercooling of e.g. 1 °C (common for most commercial alloys and castings) in the absence of inoculants, the solidification would have started at 656.8 °C and would have formed primary α -Al containing 0.061 wt.% Si and liquid containing 0.59 wt.% Si. Under this condition, using the lever rule, it can be calculated that about 34% of the primary α -Al

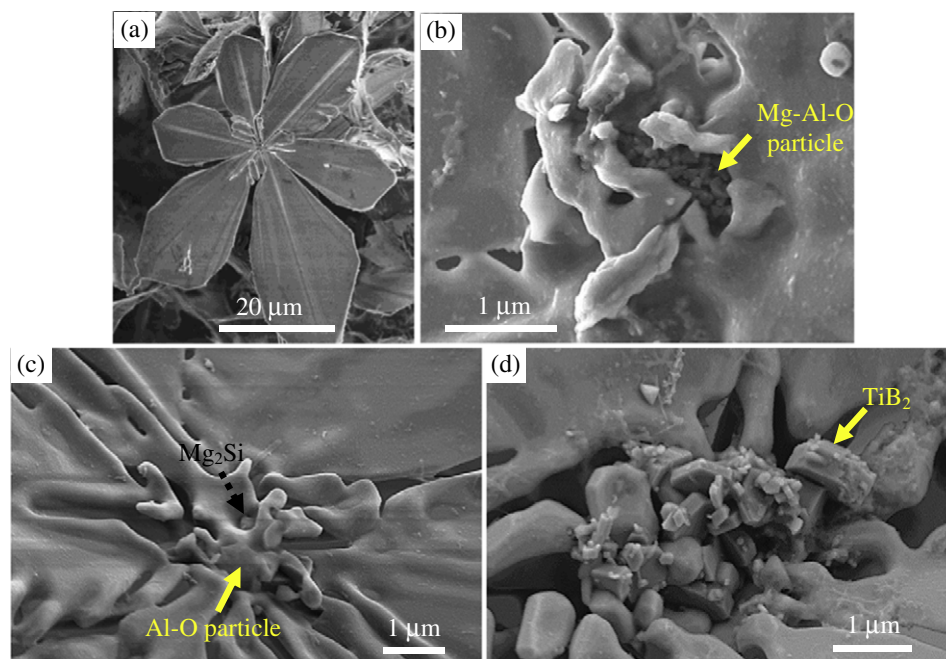


Fig. 4. FEG-SEM images of the extracted particles revealing (a) flower-like particle, and (b–d) association of Mg–Al–O rich, Al–O rich and TiB_2 particles at the centres of flower-like particles.

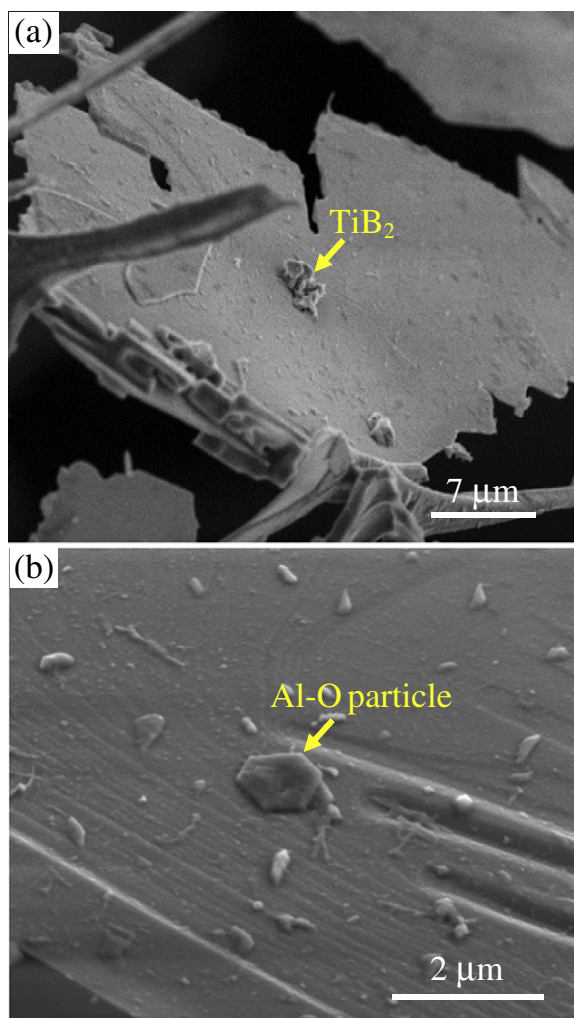


Fig. 5. FEG-SEM images of the extracted particles showing association between (a) TiB_2 , and (b) Al–O rich particles with $\beta\text{-AlFeSi}$.

solidifies. In the case of the inoculated alloy, assuming negligible undercooling, the solidification starts at the equilibrium temperature and forms primary $\alpha\text{-Al}$ containing only 0.043 wt.% Si. Such a small difference in the Si content of the initial primary $\alpha\text{-Al}$ will lead to a large difference in the composition of the last remaining liquid to solidify. Such high solute-rich liquid will therefore be more favourable for the formation of the Si-rich IMC $\beta\text{-AlFeSi}$, as observed in the GR samples. EPMA line scans across grains (shown in Fig. 9) demonstrate that the GR-ED crystals have 3 times lower Si and 2 times lower Mg content in solid solution compared to the NGR-FD crystals. The low level of Si in the $\alpha\text{-Al}$ solid solution means that higher levels of Si segregated to the grain boundaries or inter-dendritic regions (Fig. 9) which would be sufficient to promote $\beta\text{-AlFeSi}$ (the theoretical Si:Fe ratios for $\beta\text{-Al}_5\text{FeSi}$ and $\alpha\text{-Al}_8\text{Fe}_2\text{Si}$ are ~ 1 and ~ 0.5 , respectively). The average solute contents inside the grains are given in Table 3. Significant care was taken not to include the solute associated with the eutectics in the calculation. The measured Si (0.04 wt.%) and Mg (0.18 wt.%) contents of the GR-ED

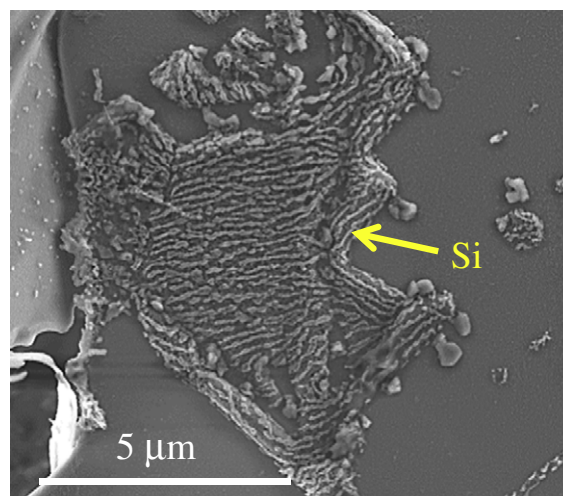


Fig. 6. FEG-SEM image showing Si particles on the surface of $\beta\text{-AlFeSi}$.

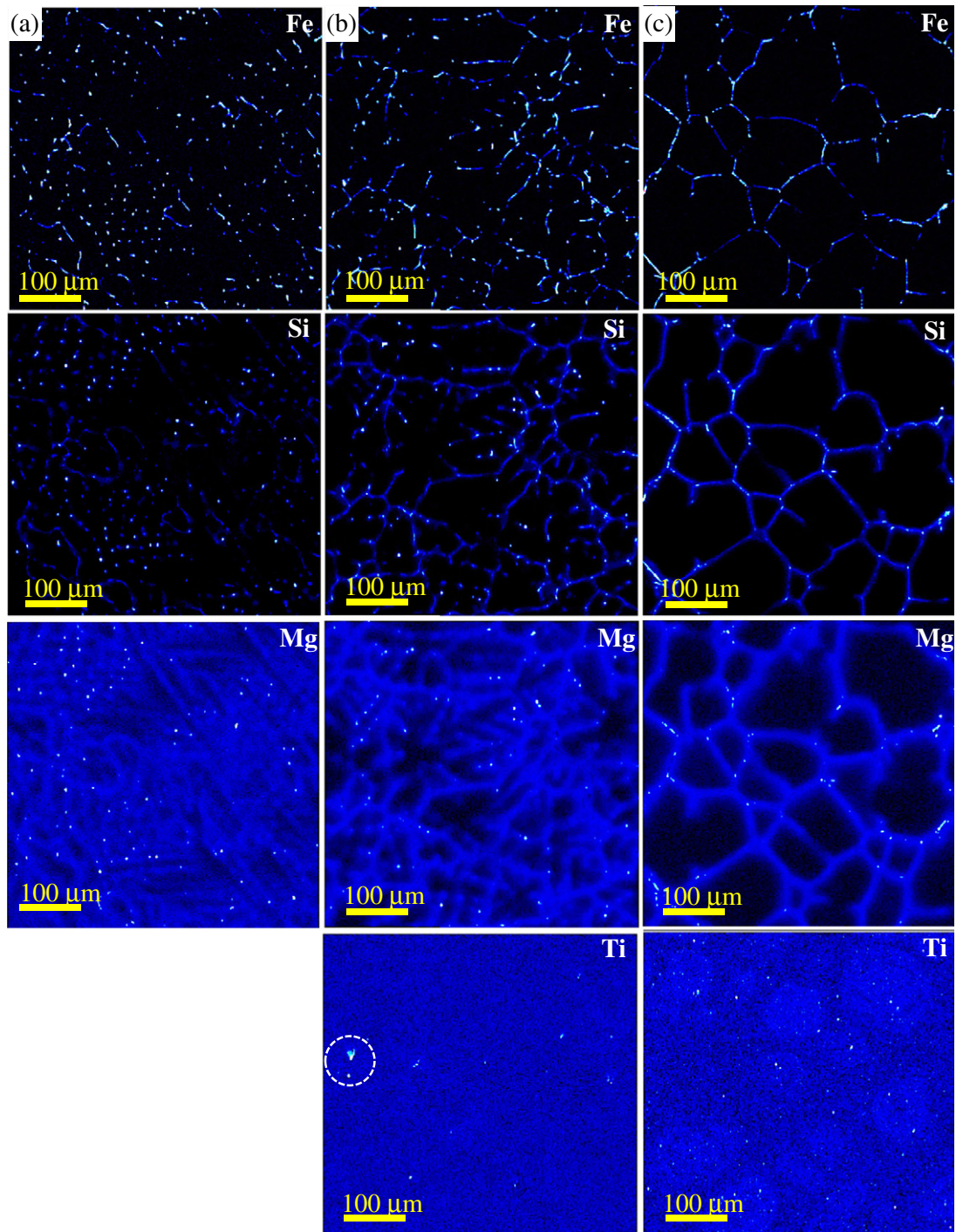


Fig. 7. EPMA maps showing Fe, Si, Mg and Ti distributions across (a) NGR-FD, (b) GR-ED and (c) GR-G samples. Fe, Si and Mg were enriched in the inter-dendritic and inter-granular regions whereas Ti was enriched within the primary α -Al solid solution. The Ti-rich particles (circled, (b)) were uniformly distributed in the GR-G sample (c).

crystals are much closer to the MTDATA predicted values (0.04 wt.% Si and 0.12 wt.% Mg) of the initial equilibrium solidified primary α -Al. It is also possible that the floating crystals that formed earlier in different parts of the sump have been transported by fluid convection to the centre of the billet during casting and contribute to lean solute concentration crystals [1]. The NGR-FG sample had only feathery columnar grains in the analysed billet (Fig. 1(a)), however the GR-ED sample had a uniform equiaxed grain structure (Fig. 1(c)) suggesting all are either native or floating crystals. Overall, the change in chemistry of the final liquid film between the grains appears to affect the intermetallic

phase selection. This effect can be attributed to the different nucleation temperatures of the primary α -Al.

4.1.2. Concerning the Primary α -Al Growth

The primary α -Al crystal morphology that develops during casting determines the position, shape and inter-connectivity of the segregated solute-rich liquid from which the Fe-IMCs form. For a given solute-rich liquid fraction, the dendritic grains distribute the liquid into finer pools compared to the globular grains. This is because the dendritic grains have both inter-dendritic and inter-granular regions over which to

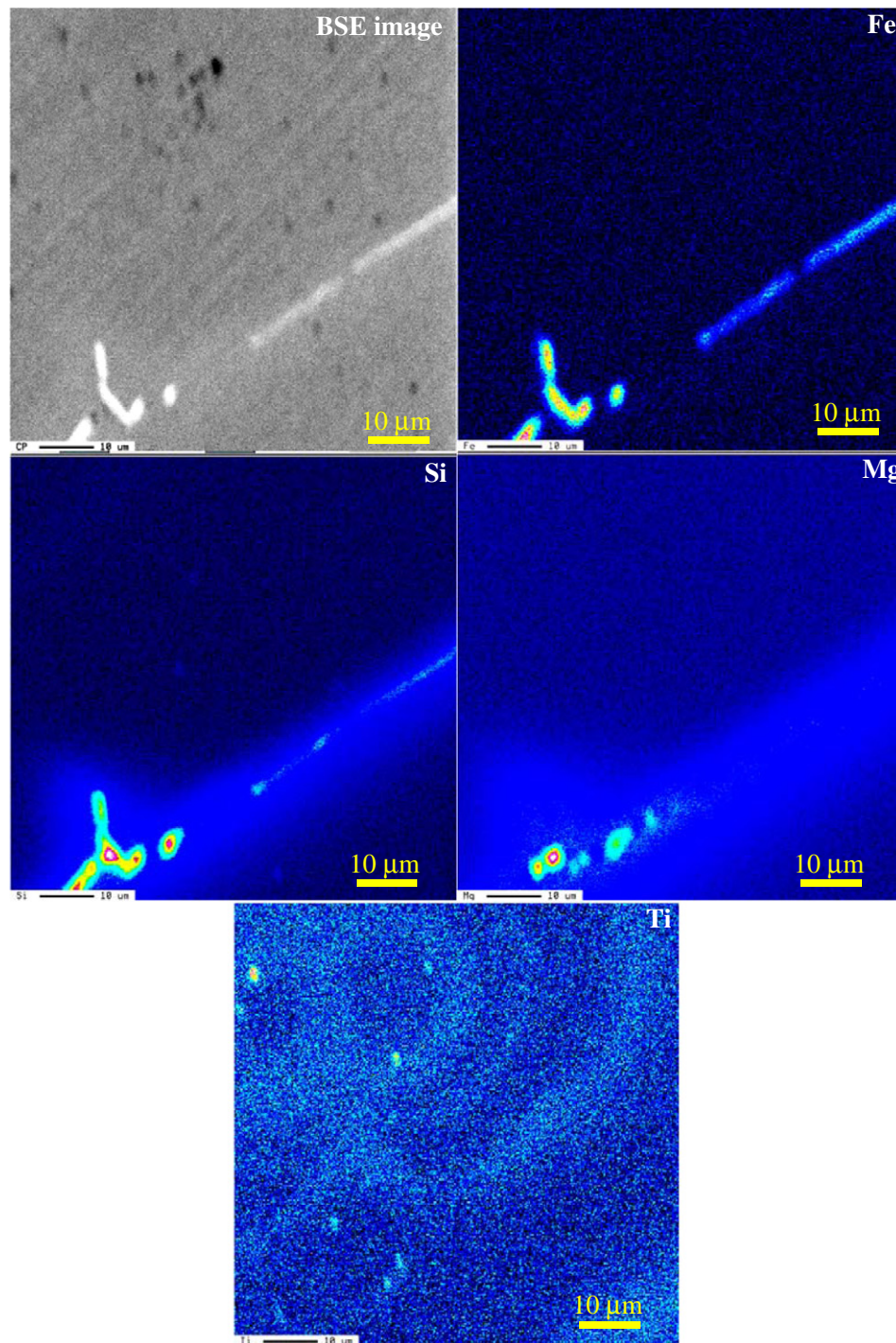


Fig. 8. EPMA maps showing the solute distributions across part of a globular grain in the GR-G sample. The solute Ti inside the grain shows ring-like patterns.

spread and distribute the given amount of liquid, whereas the globular grains accumulate the liquid only in the inter-granular regions. Therefore the feathery columnar grains which have a larger fraction of the “isolated” liquid pools (like droplets) inside the grain envelope, have less inter-connected grain boundary solute-rich liquid films, which solidify as less inter-connected Fe-IMCs (Fig. 3(a)) when compared to the equiaxed grains (Fig. 3(c) to Fig. 3(e)). IMCs which form from the liquid droplets do not connect to the inter-connected network, and remain isolated. Details of the “isolated” liquid droplet formation and solidification can be found in [42]. In addition, the growth rate of equiaxed

grains in the GR sample is slower than the columnar grains in the NGR sample [45]. Hence the Fe-IMCs that form later in the solidification sequence at the grain boundary of equiaxed (dendritic/globular) grains, have more time to grow freely and join in order to form the observed network of highly inter-connected Fe-IMCs. It is important to note that the inter-connectivity of the Fe-IMCs does not depend on the type of IMCs, rather it depends on the α -Al grain morphology and size that develop during casting. In other words, the primary α -Al growth morphology predominantly affects the inter-connectivity and size of the Fe-IMCs, rather than the type of IMC.

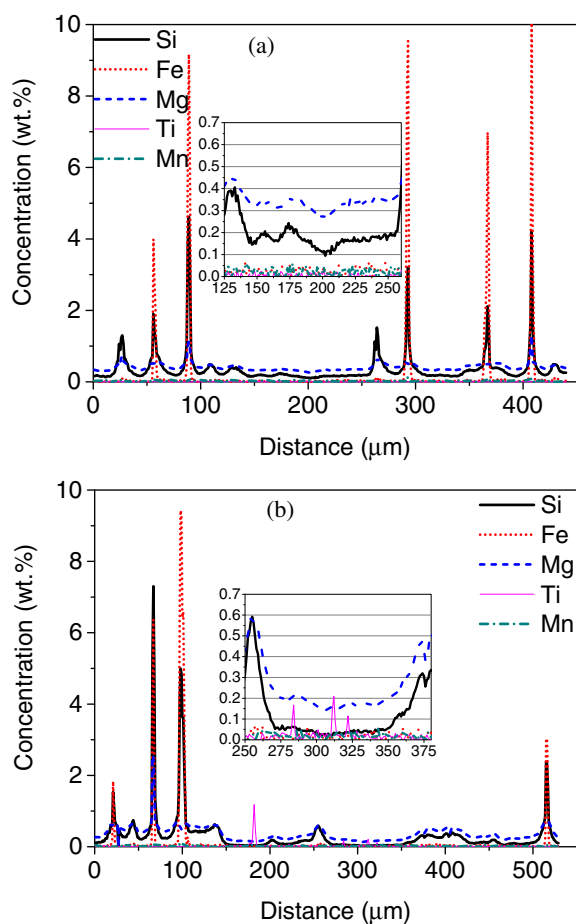


Fig. 9. Elemental line scans from EPMA of billets cast conventionally with no GR (a) and with GR (b). Inserts show enlarged regions between two eutectics.

4.2. From the Perspective of the Fe-IMCs Solidification

Since DC casting provides a cooling rate higher than equilibrium conditions [1,13,14], the secondary phases that solidify from the solute rich liquid may not be similar to those predicted by modelling. In our earlier studies it was shown that the phases formed during casting are much closer to those predicted under Scheil assumptions rather than by the lever rule [17,18,42]. The XRD analysis and SEM analysis confirmed the presence of α -AlFeSi, β -AlFeSi and Mg_2Si in all the billets, but the largest discrepancy between the prediction (under the assumptions shown in Fig. 10(a)) and experiment was $\text{Al}_{13}\text{Fe}_4$. It is possible that $\text{Al}_{13}\text{Fe}_4$ was suppressed kinetically during casting or that the fraction present was too low to detect, or more likely, formed and then transformed into α -AlFeSi and β -AlFeSi. The absence of the predicted low fraction of α -AlMnSi was again due to it either being suppressed kinetically or being too low in fraction to detect. Although Si flakes (Fig. 6) and discrete Si particles similar to those in [42] are revealed in the SEM investigations, the absence of Si in the XRD analysis is because of its low fraction. By mathematically suppressing the $\text{Al}_{13}\text{Fe}_4$ as in Fig. 10(b), the modelling predicted the types of phases seen in the experiments more closely. The scenario of α -AlFeSi and β -AlFeSi growth fronts occurring in sequence behind the primary α -Al growth fronts with different grain morphologies are also illustrated in Fig. 11.

The possible solidification reactions suggested for 6xxx series Al alloys are listed elsewhere [42]. Based on the extracted particles, complex morphologies and length scales, from thermodynamic simulations of the phase fractions as shown in Fig. 10, and from previous in-situ solidification studies [46,47], it can be inferred that most of these Fe-IMC

particles form through the following eutectic reactions: (a) $\text{L} \rightarrow \alpha\text{-Al} + \alpha\text{-AlFeSi}$, and (b) $\text{L} \rightarrow \alpha\text{-Al} + \beta\text{-AlFeSi}$ with the reaction products growing in a weakly coupled or uncoupled manner. The eutectic α -AlFeSi or β -AlFeSi component nucleates and grows separately while the eutectic Al component either (a) forms as part of the advancing/coarsening primary α -Al dendrites, or (b) nucleates on one of the nearby primary α -Al dendrites and grows with a similar orientation. Hence the following sections will deal with the nucleation and growth of the α -AlFeSi and β -AlFeSi components of the eutectic.

4.2.1. Concerning the Fe-IMCs Nucleation

IMCs with a higher nucleation temperature (small melt undercooling) form initially, followed by phases with lower nucleation temperatures [13]. As per the prediction in Fig. 10(b), the nucleation temperature of α -AlFeSi was higher than that of β -AlFeSi. Thus for the β -AlFeSi to be dominant in casting, as in the GR samples, the α -AlFeSi nucleation should be suppressed or the β -AlFeSi nucleation temperature should be raised. The high Si content of the segregated solute rich liquid in the GR samples is likely to increase the difficulty of α -AlFeSi nucleation because α -AlFeSi is less favourable than β -AlFeSi when the Si concentration is beyond ~8 wt.%, according to the Al-Fe-Si phase diagram [48]. Under such a scenario, β -AlFeSi will be nucleated at a higher temperature, as predicted in Fig. 10(c).

The observed association of oxide and TiB_2 particles with flower-like α -AlFeSi (Fig. 4) and platelet-like β -AlFeSi (Fig. 5) particles strongly suggests potential heterogeneous nucleation events are taking place. This scenario is also indicated in Fig. 11. When the Al-5Ti-1B grain refiner is added, only a few of the TiB_2 inoculants contribute to the primary α -Al nucleation [49] while the remaining unused inoculants, in the form of clusters or individual particles, are pushed to the inter-dendritic and inter-granular liquid by the growing solid-liquid interfaces. These “unused” inoculants are thus available to affect the IMCs that solidify later in the solidification. TEM analysis [15] confirmed that TiB_2 and β -AlFeSi have a good crystallographic orientation relationship. Thus β -AlFeSi which forms at a higher temperature in the GR samples as the result of the high Si segregation will be easily nucleated by TiB_2 particles even at lower undercooling, and so is even more favoured. This argument also holds for α -AlFeSi and TiB_2 , provided the local chemistry is favourable. Similar to TiB_2 , the oxide particles (such as Al_2O_3 , MgO , MgAl_2O_4 , etc.) also nucleate Fe-IMCs [46,47,50–52] and such heterogeneous nucleation will take place directly or with intermediate compounds [53–55]. However, these nucleation mechanisms need to be verified using techniques such as in-situ X-ray solidification observation, which is currently limited due to low spatial resolution [46,47].

The heterogeneous nucleation mechanism of the flower-like α -AlFeSi seems to be complex and different to that of platelet-like β -AlFeSi. It is probable, that the heterogeneous nucleation of α -AlFeSi resulted in a coupled binary eutectic reaction (as stated earlier) or a coupled ternary eutectic reaction ($\text{L} \rightarrow \alpha\text{-Al} + \alpha\text{-AlFeSi} + \text{Mg}_2\text{Si}$) leading to a lamella-like appearance at the centre (Fig. 4) after which petals develop and grow outwards. Occasionally, fine Mg_2Si particles can be observed close to the originating point of α -AlFeSi as shown in Fig. 4(c), suggesting the above ternary eutectic reaction. β -AlFeSi seems to heterogeneously nucleate and grow throughout in an uncoupled manner. Overall, the potent nucleant particles aid the nucleation of Fe-IMCs. However, the type of Fe-IMCs they nucleate/select, will depend upon the local chemistry and thermal conditions in the liquid film.

4.2.2. Concerning the Fe-IMCs Growth

If two IMCs nucleate at two different temperatures, the IMC with higher growth temperature (higher growth velocity) will dominate in the casting by suppressing the other IMC [13]. The growth of α -AlFeSi and β -AlFeSi will be affected by the local chemistry of the liquid in which they grow. In addition, the growth shape of the Fe-IMC particles is a function of the grain structure.

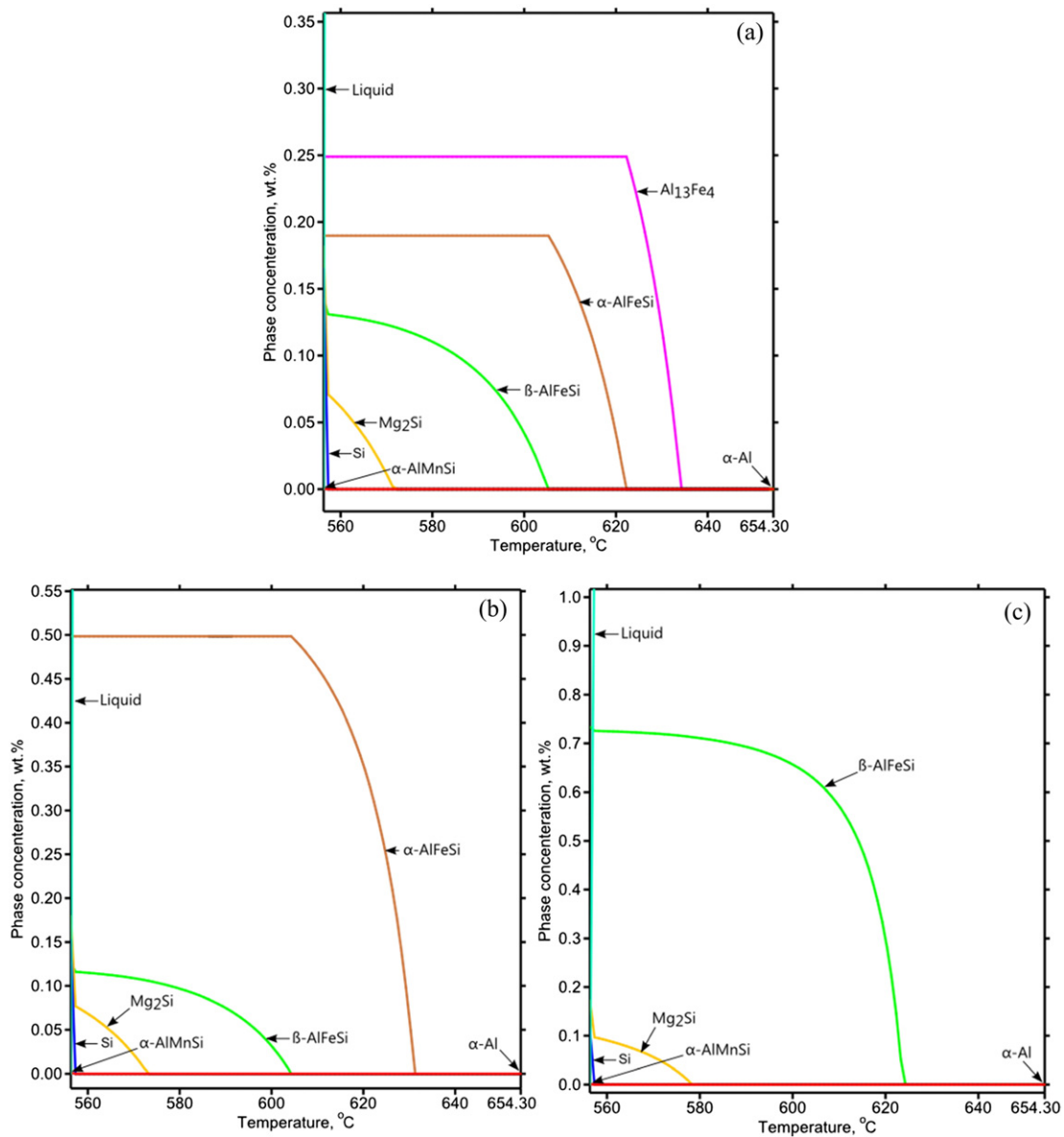


Fig. 10. Thermodynamic calculations of phase fractions for the batch 1 6063 alloy, assuming Scheil solidification conditions, where (a) has no phases suppressed, (b) has $\text{Al}_{13}\text{Fe}_4$ suppressed, and (c) has $\text{Al}_{13}\text{Fe}_4$ and $\alpha\text{-AlFeSi}$ suppressed.

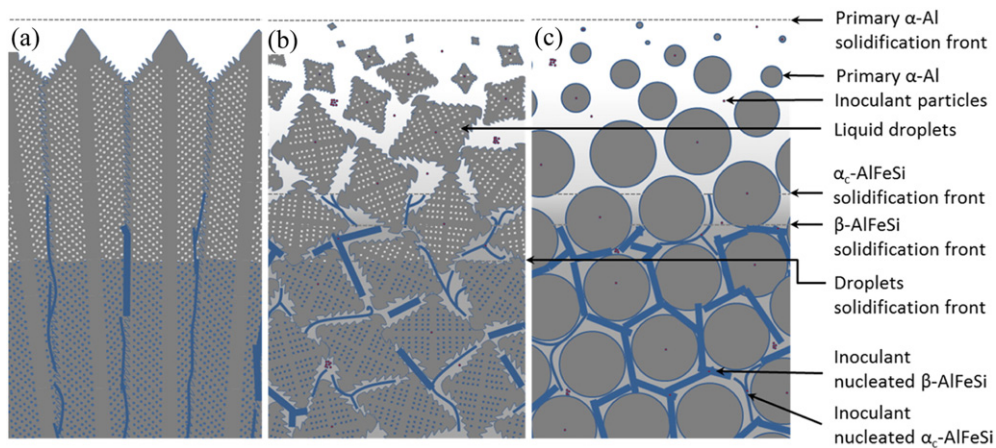


Fig. 11. Schematic representation of the solidification sequences in 6063 billet during DC casting for different primary $\alpha\text{-Al}$ morphologies, (a) feathery-dendritic, (b) equiaxed dendritic, and (c) equiaxed-globular $\alpha\text{-Al}$ grains respectively.

Table 3

The average lower content of different solutes, in the solid solution of Al, in conventionally DC cast samples.

Sample	Si (wt.%)	Mg (wt.%)	Fe (wt.%)	Mn (wt.%)
NGR-FD	0.16 ± 0.02	0.32 ± 0.02	0.02 ± 0.01	0.01 ± 0.01
GR-ED	0.04 ± 0.01	0.18 ± 0.02	0.01 ± 0.01	0.01 ± 0.01

For the reasons stated in the earlier article [17], the cubic α -AlFeSi particles can easily adapt and grow into different shapes based on the “constrained” shape of the liquid. Here “constrained” refers to the isolated solute-rich liquid droplets or channels surrounding the α -Al. For example, the α -AlFeSi particles adapt to grow with a skeleton-like (Fig. 3(a)) morphology when the liquid channel is thin, and with a rosette-like [42] or blocky-like [56] morphology when the liquid is in a spherical droplet form. The α -AlFeSi particles grow and coarsen (Fig. 3(b)) if the liquid film around the grains are thick, as in the NGR-G structured sample. The fully developed “6 petal” flower-like α -AlFeSi particles in the inter-granular region of the globular grains, implies that these particles nucleate and grow from liquid, which had a uniform temperature and little physical constraint. The transition from lamella (coupled eutectic) to petals (similar to primary α -AlFeSi dendrites) in the centre of flower-like particles occurs when the eutectic Al component finds it difficult to grow in a coupled manner.

The monoclinic β -AlFeSi particles which have a faceted interface with the liquid Al usually thicken via step or re-entrant edge mechanisms giving defined platelet-like or rack-like morphologies (Fig. 3(c,d)). Unlike α -AlFeSi, β -AlFeSi seems to have similar morphologies (usually platelets) whether they form within a constrained volume of liquid such as spherical droplets [53] or in the grain boundary liquid film. The evidence of the platelet-like β -AlFeSi particle with ledges growing over the petal of the flower-like α -AlFeSi particle in Fig. 3(e) suggests that the α -AlFeSi formed at a higher temperature prior to the β -AlFeSi and both impinged during growth. This agrees well with the thermodynamic modelling (Fig. 10) which predicted α -AlFeSi forming at a higher temperature prior to β -AlFeSi during solidification. Both the Fe-IMCs grow at inclined angles by branching, bending or climbing in order to overcome the “physical barriers” and to accommodate the convoluted shapes of the liquid films. This is also illustrated in Fig. 11. The “physical barriers” could be pre-formed α -Al dendrites, pre-formed Fe-IMCs or solid inclusions. Overall, the Fe-IMCs growth mechanisms are dictated by the primary α -Al grain morphology and local liquid chemistry, which in turn affect the size, shape and type of Fe-IMCs.

These insights are summarised schematically in Fig. 11. It is suggested that globular α -Al grains lead to an extended network of highly inter-connected coarse Fe-IMCs as a result of a well inter-connected inter-granular liquid film network. Since these continuous networks of brittle IMCs are detrimental to the downstream deformation processes and final product [12], it is necessary to avoid their formation by promoting dendritic grains in castings, resulting in fine and less inter-connected IMCs. Fine and discrete IMCs in billets are more favourable for downstream processing stages and lead to well distributed Fe-IMCs particles in the final finished product [10,12]. Having a high fraction of inter-connected coarse α -AlFeSi in the cast billets is also harder to break-up during homogenisation (as they are thermodynamically stable, and require longer homogenisation temperatures and times) [42], therefore it is advantageous to have a relatively high fraction of β -AlFeSi (as β -AlFeSi is a metastable low temperature phase in this alloy) which more easily transform into fine α -AlFeSi particles at relatively shorter homogenisation times and lower temperatures.

5. Conclusions

Near industrial scale billets with different primary α -Al grain structures have been successfully produced with and without (i) a commercial Al-5Ti-1B grain refiner addition and (ii) intensive melt shearing. The

grain refiner addition and intensive shearing both refined the α -Al grain size significantly. “ α -AlFeSi” and “ β -AlFeSi” are the two main Fe-IMCs in these billets. The inter-connectivity, shape and size of the IMCs are all governed by the shape of the solute-rich liquid region which inherently depends on the primary α -Al morphology. A coarse feathery α -Al grain structure resulted in a network of less inter-connected Fe-IMCs, while fine globular and fine dendritic equiaxed structures resulted in a network of highly inter-connected Fe-IMCs. The Fe-IMC types do not affect the inter-connectivity. During growth, since α -AlFeSi and β -AlFeSi can bend, branch and/or climb easily during growth, the changes in the α -Al grain structure (grain morphology and grain size) do not affect the phase selection. This disproves the concept of phase selection induced by changing the primary α -Al structures.

It has been reconfirmed that TiB₂ based grain refiner additions affects the intermetallic phase selection and this is irrespective of the α -Al grain structure which is present. Al-5Ti-1B grain refiner led to β -AlFeSi phase selection, while α -AlFeSi was favoured in the billets without grain refiner. The observation of TiB₂ and oxide particles in the vicinity of α -AlFeSi and β -AlFeSi particles suggests possible heterogeneous nucleation events. The combined availability of favourable solute rich liquid and potent heterogeneous nucleating particles, promotes β -AlFeSi to form in larger proportions in the alloys containing grain refiner additions. In summary, the current study has clearly shown that Al-Ti-B grain refiner controls the Fe-IMC phase selection, and α -Al grain size and morphology affects the Fe-IMCs morphology.

Acknowledgement

The authors acknowledge the financial support of the UK Engineering and Physical Science Research Council (EPSRC grants: Centre for Innovative Manufacturing Research on Liquid Metal Engineering, EP/H026177/1, and Impact Acceleration Account Award, EP/K503769/1), and SAPA, UK. Authors acknowledge Mr. C. Salter of Oxford University for help with the EPMA and Mr. S. Jones, Dr. H.T. Li, Dr. J.B. Patel and Professor Z. Fan of Brunel University supplying the high shearing equipment and for help with the DC casting.

References

- [1] D.G. Eskin, *Physical Metallurgy of Direct Chill Casting of Aluminum Alloys*, CRC Press/Taylor & Francis, Boca Raton, 2008.
- [2] H. Zhu, X. Zhang, M. Couper, A. Dahle, Effect of initial microstructure on surface appearance of anodized aluminum extrusions, *Metall. Mater. Trans. A* 40 (2009) 3264–3275.
- [3] Y. Ma, X. Zhou, G.E. Thompson, J.O. Nilsson, M. Gustavsson, A. Crispin, Anodizing of AA6063 aluminum alloy profiles: generation of dark appearance, *Surf. Interface Anal.* 45 (2013) 1479–1484.
- [4] J. Sarkar, T.R.G. Kutty, D.S. Wilkinson, J.D. Embury, D.J. Lloyd, Tensile properties and bendability of T4 treated AA6111 aluminum alloys, *Mater. Sci. Eng. A* 369 (2004) 258–266.
- [5] Y. Shen, T.F. Morgeneyer, J. Garnier, L. Allais, L. Helfen, J. Crépin, Three-dimensional quantitative in situ study of crack initiation and propagation in AA6061 aluminum alloy sheets via synchrotron laminography and finite-element simulations, *Acta Mater.* 61 (2013) 2571–2582.
- [6] S. Onurlu, A. Tekin, Effect of heat treatment on the insoluble intermetallic phases present in an AA 6063 alloy, *J. Mater. Sci.* 29 (1994) 1652–1655.
- [7] S. Zajac, B.B. Hutchinson, A.A. Johansson, L.Q.L.-O. Gullman, Microstructure control and extrudability of Al-Mg-Si alloys microalloyed with manganese, *Mater. Sci. Technol.* 10 (1994) 323–333.
- [8] M.H. Mulazimoglu, A. Zaluska, J.E. Gruzleski, F. Paray, Electron microscope study of Al-Fe-Si intermetallics in 6201 aluminum alloy, *Metall. Mater. Trans. A Phys. Metall. Mater. Sci.* 27 (1996) 929–936.
- [9] F.H. Samuel, A.M. Samuel, H.W. Doty, S. Valtierra, Decomposition of Fe-intermetallics in Sr-modified cast 6XXX type aluminum alloys for automotive skin, *Metall. Mater. Trans. A Phys. Metall. Mater. Sci.* 32 (2001) 2061–2075.
- [10] S. Kumar, N.H. Babu, G.M. Scamans, Z. Fan, Influence of intensive melt shearing on the microstructure and mechanical properties of an Al-Mg alloy with high added impurity content, *Metall. Mater. Trans. A Phys. Metall. Mater. Sci.* 42A (2011) 3141–3149.
- [11] S. Kumar, N.H. Babu, G.M. Scamans, Z. Fan, Microstructural evaluation of melt conditioned twin roll cast Al-Mg alloy, *Mater. Sci. Technol.* 27 (2011) 1833–1839.
- [12] S. Kumar, N. Hari Babu, G.M. Scamans, Z. Fan, K.A.Q. O'Reilly, Twin roll casting of Al-Mg alloy with high added impurity content, *Metall. Mater. Trans. A* (2014) 2842–2854.

- [13] C.M. Allen, K.A.Q. O'Reilly, B. Cantor, P.V. Evans, Intermetallic phase selection in 1XXX Al alloys, *Prog. Mater. Sci.* 43 (1998) 89–170.
- [14] Y.L. Liu, S.B. Kang, H.W. Kim, The complex microstructures in an as-cast Al–Mg–Si alloy, *Mater. Lett.* 41 (1999) 267–272.
- [15] G. Sha, K. O'Reilly, B. Cantor, R. Hamerton, J. Worth, Effect of grain refiner on intermetallic phase formation in directional solidification of 6xxx series wrought Al alloys, *Mater. Sci. Forum* 331 (2000) (1/).
- [16] G. Sha, K. O'Reilly, B. Cantor, J. Worth, R. Hamerton, Growth related metastable phase selection in a 6xxx series wrought Al alloy, *Mater. Sci. Eng. A* 304–306 (2001) 612–616.
- [17] A. Verma, S. Kumar, P.S. Grant, K.A.Q. O'Reilly, Influence of cooling rate on the Fe intermetallic formation in an AA6063 Al alloy, *J. Alloys Compd.* 555 (2013) 274–282.
- [18] T. Smith, K. O'Reilly, S. Kumar, I. Stone, Influence of grain-refiner addition on the morphology of Fe-bearing intermetallics in a semi-solid processed Al–Mg–Si alloy, *Metall. Mater. Trans. A Phys. Metall. Mater. Sci.* 44 (2013) 4866–4871.
- [19] C. Brito, T.A. Costa, T.A. Vida, F. Bertelli, N. Cheung, J.E. Spinelli, A. Garcia, Characterization of dendritic microstructure, intermetallic phases, and hardness of directionally solidified Al–Mg and Al–Mg–Si alloys, *Metall. Mater. Trans. A* 46 (2015) 3342–3355.
- [20] S.J. Maggs, *School of Materials*, Vol. Ph.D. Leeds: The University of Leeds, 1996.
- [21] M.W. Meredith, A.L. Greer, P.V. Evans, in: W. BJ (Ed.), *The Effect of Grain-refining Additions on Intermetallic Selection in Dilute Aluminum Alloys*, The Minerals, Metals and Materials Society, San Antonio, TX, USA 1998, pp. 977–982 (The Minerals, Metals and Materials Society: San Antonio, TX, USA).
- [22] X.G. Chen, Effect of Grain Refiners on Intermetallic Phases in AA1xxx Simulated DC Castings, *Proceedings of the 128th TMS Annual Meeting 'Light Metals'*, San Diego; CA, USA 1999, pp. 803–809.
- [23] M.W. Meredith, A.L. Greer, P.V. Evans, The Influence of Grain Refiner on Intermetallic Phase Selection in Dilute Al–Fe Alloys, *Proceedings of the 4th Decennial International Conference on Solidification Processing* 1997, pp. 541–545.
- [24] M.W. Meredith, A.L. Greer, P.V. Evans, R.G. Hamerton, Generation of Al mFe in Dilute Aluminum Alloys with Different Grain Refining Additions, *Proceedings of the 128th TMS Annual Meeting 'Light Metals'*, San Diego CA, USA 1999, pp. 811–817.
- [25] G.I. Eskin, I.N. Friedlyander, Crystallization of aluminum–copper alloys as a result of ultrasonic oscillation, *Met. Sci. Heat Treat.* 4 (1962) 154–157.
- [26] M.D. Sahu, V.A. Gadgil, Effects of electromagnetic fields on solidification of some aluminium alloys, *Br. Foundryman* 70 (1977) 89–92.
- [27] Y. Osawa, S. Takamori, T. Kimura, K. Minagawa, H. Kakisawa, Morphology of intermetallic compounds in Al–Si–Fe alloy and its control by ultrasonic vibration, *Mater. Trans.* 48 (2007) 2467–2475.
- [28] X. Li, Z. Ren, Y. Fautrelle, Y. Zhang, C. Esling, Morphological instabilities and alignment of lamellar eutectics during directional solidification under a strong magnetic field, *Acta Mater.* 58 (2010) 1403–1417.
- [29] J.B. Patel, H.T. Li, M.X. Xia, S. Jones, S. Kumar, K. O'Reilly, Z.Y. Fan, Melt Conditioned Direct Chill Casting (MC-DC) Process for Production of High Quality Aluminium Alloy Billets. 14th International Conference on Aluminium Alloys, ICAA 2014, vol. 794–796, Trondheim: Trans Tech Publications Ltd, 2014, p.149–154.
- [30] J. Barbosa, H. Puga, J. Oliveira, S. Ribeiro, M. Prokic, Physical modification of intermetallic phases in Al–Si–Cu alloys, *Mater. Chem. Phys.* 148 (2014) 1163–1170.
- [31] L.-Y. Chen, J.-Q. Xu, H. Choi, H. Konishi, S. Jin, X.-C. Li, Rapid control of phase growth by nanoparticles, *Nat. Commun.* 5 (2014) 3879.
- [32] P. Mikolajczak, L. Ratke, Interplay between melt flow and the 3D distribution and morphology of Fe-rich phases in AlSi alloys, *Metall. Mater. Trans. A* 46 (2015) 1312–1327.
- [33] Z. Fan, Y.B. Zuo, B. Jiang, Apparatus and method for liquid metals treatment, UK (2010).
- [34] L.B. Ber, *X-Ray Diffraction (Part II)*, Taylor and Francis, 2005.
- [35] P.R. Goulart, V.B. Lazarine, C.V. Leal, J.E. Spinelli, N. Cheung, A. Garcia, Investigation of intermetallics in hypoeutectic Al–Fe alloys by dissolution of the Al matrix, *Intermetallics* 17 (2009) 753–761.
- [36] S. Henry, T. Minghetti, M. Rappaz, Dendrite growth morphologies in aluminium alloys, *Acta Mater.* 46 (1998) 6431–6443.
- [37] L. Bäckerud, E. Król, J. Tamminen, *Solidification Characteristics of Aluminium Alloys: Wrought Alloys*, 1986.
- [38] E. Liotti, A. Lui, R. Vincent, S. Kumar, Z. Guo, T. Connolly, I.P. Dolbnya, M. Hart, L. Arberg, R.H. Mathiesen, P.S. Grant, A synchrotron X-ray radiography study of dendrite fragmentation induced by a pulsed electromagnetic field in an Al–15Cu alloy, *Acta Mater.* 70 (2014) 228–239.
- [39] H.T. Li, Y. Wang, Z. Fan, Mechanisms of enhanced heterogeneous nucleation during solidification in binary Al–Mg alloys, *Acta Mater.* 60 (2012) 1528–1537.
- [40] A. Das, S. Ji, Z. Fan, Morphological development of solidification structures under forced fluid flow: a Monte-Carlo simulation, *Acta Mater.* 50 (2002) 4571–4585.
- [41] S. Kumar, P.S. Grant, K.A.Q. O'Reilly, Fe bearing intermetallic phase formation in a wrought Al–Mg–Si alloy, *T Indian I Metals* 65 (2012) 553–557.
- [42] S. Kumar, P.S. Grant, K.A.Q. O'Reilly, Evolution of Fe bearing intermetallics during DC casting and homogenization of an Al–Mg–Si alloy, *Metall. Mater. Trans. A* 47 (2016) 3000–3014.
- [43] M. Rappaz, J. Friedli, A. Mariaux, M. Salgado-Ordorica, The influence of solid–liquid interfacial energy anisotropy on equilibrium shapes, nucleation, triple lines and growth morphologies, *Scr. Mater.* 62 (2010) 904–909.
- [44] M.A. Salgado-Ordorica, P. Burdet, M. Cantoni, M. Rappaz, Study of the twinned dendrite tip shape II: experimental assessment, *Acta Mater.* 59 (2011) 5085–5091.
- [45] X. Yao, S.D. McDonald, A.K. Dahle, C.J. Davidson, D.H. StJohn, Modeling of grain refinement: part III. Al–7Si–0.3Mg aluminum alloy, *J. Mater. Res.* 23 (2008) 1301–1306.
- [46] S. Terzi, J.A. Taylor, Y.H. Cho, L. Salvo, M. Suéry, E. Boller, A.K. Dahle, In situ study of nucleation and growth of the irregular α -Al/ β -Al₅FeSi eutectic by 3-D synchrotron X-ray microtomography, *Acta Mater.* 58 (2010) 5370–5380.
- [47] C. Puncrobut, A.B. Phillion, J.L. Fife, P. Rockett, A.P. Horsfield, P.D. Lee, In situ quantification of the nucleation and growth of Fe-rich intermetallics during Al alloy solidification, *Acta Mater.* 79 (2014) 292–303.
- [48] N.A. Belov, A.A. Aksenov, D.G. Eskin, *Iron in Aluminium Alloys: Impurity and Alloying Element*, Taylor & Francis, 2002.
- [49] A.L. Greer, P.S. Cooper, M.W. Meredith, W. Schneider, P. Schumacher, J.A. Spittle, A. Tronche, Grain refinement of aluminium alloys by inoculation, *Adv. Eng. Mater.* 5 (2003) 81–91.
- [50] X. Cao, J. Campbell, The nucleation of Fe-rich phases on oxide films in Al–11.5Si–0.4 Mg cast alloys, *Metall. Mater. Trans. A* 34 (2003) 1409–1420.
- [51] W. Khalifa, F.H. Samuel, U. Gm Nserc, J.E. Gruzleski, H.W. Doty, S. Valtierra, Nucleation of Fe-intermetallic phases in the Al–Si–Fe alloys, *Metall. Mater. Trans. A* 36 (2005) 1017–1032.
- [52] D.N. Miller, L. Lu, A.K. Dahle, The role of oxides in the formation of primary iron intermetallics in an Al–11.6Si–0.37Mg alloy, *Metall. Mater. Trans. B* 37 (2006) 873–878.
- [53] C. Hsu, Department of Materials, University of Oxford, Oxford, 1999 (this is a DPhil thesis).
- [54] P. Cizek, B.J. McKay, S. Lozano-Perez, Investigation of the interfaces between boride particles and aluminium in the as-received and re-melted Ti–B–Al grain refiner master alloy, *Inst. Phys. Conf. Ser.* 179 (2004) 429–432.
- [55] V. Srinivas, V. Singh, Development of in situ as cast Al–Mg₂Si particulate composite: microstructure refinement and modification studies, *T Indian I Metals* 65 (2012) 759–764.
- [56] C. Hsu, K.A.Q. O'Reilly, B. Cantor, R. Hamerton, Non-equilibrium reactions in 6xxx series Al alloys, *Mater. Sci. Eng. A* 304–306 (2001) 119–124.